

Enhancing thermodynamic performances and suppressing fluctuations in interacting quantum-dot thermoelectric engines

Jianhan Zhuang(庄剑涵), Qinyan Zou(邹沁研), Ziming Wang(王子明), Gaoyuan Chen(陈高远), Jian Sun(孙坚), Xiang Hao(郝翔), Chen Wang(王晨), and Jincheng Lu(陆金成)

Citation: Chin. Phys. B, 2026, 35 (**1**): 010508. DOI: 10.1088/1674-1056/ae12de
http://cpb.iphy.ac.cn; http://iopscience.iop.org/cpb

What follows is a list of articles you may be interested in

Chaos of cavity optomechanical system with Coulomb coupling

Yingjia Yang(杨应佳), Liwei Liu(刘利伟), Lianchun Yu(俞连春), Weizheng Kong(孔伟正), Haiyan Jiao(焦海燕), Xiaoyan Deng(邓小燕), and Xiaoyong Li(李小勇)

Chin. Phys. B, 2025, 34 (**8**): 080503. DOI: 10.1088/1674-1056/add509

Two innovative equivalent statements of the third law of thermodynamics

Xiaohang Chen(陈晓航), Yinghui Zhou(周颖慧), and Jincan Chen(陈金灿)|

Chin. Phys. B, 2024, 33 (**6**): 060504. DOI: 10.1088/1674-1056/ad39c8

Nonequilibrium free energy and information flow of a double quantum-dot system with Coulomb coupling

Zhiyuan Lin(林智远), Tong Fu(付彤), Juying Xiao(肖菊英), Shanhe Su(苏山河), Jincan Chen(陈金灿), and Yanchao Zhang(张艳超)

Chin. Phys. B, 2021, 30 (**8**): 080501. DOI: 10.1088/1674-1056/abe119

Numerical investigation on photonic microwave generation by a sole excited-state emitting quantum dot laser with optical injection and optical feedback

Zai-Fu Jiang(蒋再富), Zheng-Mao Wu(吴正茂), Wen-Yan Yang(杨文艳), Chun-Xia Hu(胡春霞), Yan-Hong Jin(靳艳红), Zhen-Zhen Xiao(肖珍珍), and Guang-Qiong Xia(夏光琼)

Chin. Phys. B, 2021, 30 (**5**): 050504. DOI: 10.1088/1674-1056/abd2a8

Impact of counter-rotating-wave term on quantum heat transfer and phonon statistics in nonequilibrium qubit-phonon hybrid system

Chen Wang(王晨), Lu-Qin Wang(王鲁钦), and Jie Ren(任捷)

Chin. Phys. B, 2021, 30 (**3**): 030506. DOI: 10.1088/1674-1056/abcfa8

Enhancing thermodynamic performances and suppressing fluctuations in interacting quantum-dot thermoelectric engines

Jianhan Zhuang(庄剑涵)[1,2], Qinyan Zou(邹沁研)[1,2], Ziming Wang(王子明)[1,2], Gaoyuan Chen(陈高远)[1,2], Jian Sun(孙坚)[1,2], Xiang Hao(郝翔)[1,2], Chen Wang(王晨)[3,†], and Jincheng Lu(陆金成)[1,2,‡]

[1] *Key Laboratory of Intelligent Optoelectronic Devices and Chips of Jiangsu Higher Education Institutions, School of Physical Science and Technology, Suzhou University of Science and Technology, Suzhou* 215009, *China*

[2] *Advanced Technology Research Institute of Taihu Photon Center, School of Physical Science and Technology, Suzhou University of Science and Technology, Suzhou* 215009, *China*

[3] *Department of Physics, Zhejiang Normal University, Jinhua* 321004, *China*

(Received 8 September 2025; revised manuscript received 10 October 2025; accepted manuscript online 14 October 2025)

Quantum dot systems emerge as promising platforms for studying nanoscale thermoelectric effects and quantum fluctuation phenomena. In this work, we investigate the thermodynamic performance of a Coulomb-blockaded quantum dot operating as a quantum heat engine using the quantum master equation approach. By incorporating full counting statistics, we analyze both average transport properties and current fluctuations in this nanoscale system. We demonstrate that electron–electron interactions significantly enhance thermoelectric performance by increasing both the output power and energy conversion efficiency. Furthermore, we show that Coulomb interactions suppress current fluctuations while preserving the validity of the thermodynamic uncertainty relation. Our results provide important insights into the interplay between quantum effects and thermodynamic principles in nanoscale heat engines.

Keywords: quantum dot, thermoelectric engine, Coulomb interaction, current fluctuations, thermodynamic uncertainty relation

PACS: 05.70.Ln, 05.40.Ca, 73.23.Hk, 73.50.Lw, 84.60.Rb

DOI: 10.1088/1674-1056/ae12de **CSTR:** 32038.14.CPB.ae12de

1. Introduction

The pursuit of high-efficiency quantum thermal machines has emerged as a vibrant frontier at the intersection of quantum thermodynamics and mesoscopic physics.[1–4] Quantum dot (QD) systems, with their discrete energy levels and tunable electronic properties, have proven to be exceptional platforms for exploring fundamental thermodynamic principles at the nanoscale.[5–8] These systems offer unprecedented control over electron transport and energy conversion processes, making them ideal candidates for investigating quantum-enhanced thermoelectric effects.[9–13]

Recent advances in nanofabrication techniques have enabled the experimental realization of single-electron devices operating in the Coulomb blockade regime, where electron–electron interactions play a crucial role in governing transport properties.[14–19] The strong Coulomb repulsion in these systems leads to correlated electron behavior that can significantly modify the thermoelectric response, offering opportunities for enhancing energy conversion performance beyond what is achievable in non-interacting systems. Understanding how these quantum correlations affect both average transport characteristics and fluctuation properties is essential for designing efficient quantum thermal devices.[20–22]

Furthermore, the emerging field of quantum fluctuations has revealed fundamental bounds on energy conversion processes, particularly through thermodynamic uncertainty relations (TURs) that establish intrinsic trade-offs between current fluctuations and entropy production.[23–28] While these relations have been extensively studied in classical systems, their validity and implications in strongly correlated quantum systems remain an active area of investigation. The quantum dot heat engine provides an ideal testbed for exploring these fundamental limits in the quantum regime.

In this work, we present a comprehensive theoretical investigation of a Coulomb-blockaded QD system operating as a thermoelectric heat engine. Using the quantum master equation approach combined with full counting statistics, we systematically analyze how electron–electron interactions influence both the average thermodynamic performance and current fluctuations. We demonstrate that Coulomb correlations not only enhance the output power and efficiency but also suppress current fluctuations while preserving the validity of thermodynamic uncertainty relations. Our findings provide valuable insights into the optimization of quantum thermoelectric devices and contribute to the fundamental understanding of nonequilibrium thermodynamics in nanoscale systems.

The paper is organized as follows. Section 2 details our interacting QD model and methods, Section 3 presents our re-

†Corresponding author. E-mail: wangchen@zjnu.cn

‡Corresponding author. E-mail: jinchenglu@usts.edu.cn

© 2026 Chinese Physical Society and IOP Publishing Ltd. All rights, including for text and data mining, AI training, and similar technologies, are reserved.

sults and discussion, and we conclude in Section 4.

2. Model and methods

2.1. The interacting QD systems

We investigate a single electrically defined QD operating in the Coulomb-blockade regime, which is coupled to two electronic leads, as schematically illustrated in Fig. 1. The total Hamiltonian describing the system, which includes the QD, the reservoirs (leads), and the interaction terms, can be expressed as

$$\hat{H} = \hat{H}_{\rm S} + \hat{H}_{\rm B} + \hat{H}_{\rm I}, \tag{1}$$

where the individual components are as follows:

$$\hat{H}_{\rm S} = \sum_{\sigma=\uparrow,\downarrow} \varepsilon_\sigma \hat{c}^\dagger_\sigma \hat{c}_\sigma + U \hat{c}^\dagger_\uparrow \hat{c}_\uparrow \hat{c}^\dagger_\downarrow \hat{c}_\downarrow. \tag{2}$$

This term, $\hat{H}_{\rm S}$, represents the QD internal electronic structure, with $\hat{c}^\dagger_\sigma$ and $\hat{c}_\sigma$ denoting the electron creation and annihilation operators for spin σ ($\sigma = \uparrow, \downarrow$), respectively. The energy levels of the dot are denoted by $\varepsilon_\uparrow$ and $\varepsilon_\downarrow$, corresponding to the spin-up and spin-down states. U is the electron–electron interaction.

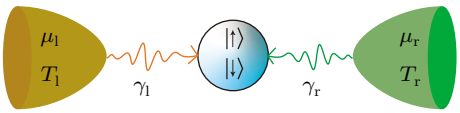


Fig. 1. Sketch of the model: a QD with spin-up and spin-down states, coupled to hot and cold reservoirs via selective transitions, operates as a thermoelectric heat engine. An electron initially tunnels from the left reservoir into the QD, occupying either the spin-up or spin-down state, characterized by the energy level ε_σ ($\sigma = \uparrow, \downarrow$). Subsequently, the electron undergoes a transition to the right reservoir. An external magnetic field tunes the system into the sequential-tunneling regime, where the QD effectively functions as a spin filter. The resulting spin blockade, which restricts electron transport, can be lifted by the hyperfine interaction between the QD electron and the nuclear spins in the surrounding host material. In this setup, the two reservoirs are characterized by different temperatures and chemical potentials: the left and right reservoirs have temperatures $T_{\rm l(r)}$ and chemical potentials $\mu_{\rm l(r)}$, respectively.

The QD is coupled to two electronic reservoirs, commonly referred to as the left (l) and right (r) leads, which enable energy exchange between the QD and its surroundings. The Hamiltonian describing these reservoirs is given by

$$\hat{H}_{\rm B} = \sum_{k,\sigma,v={\rm l,r}} \varepsilon^v_{k\sigma} \hat{d}^\dagger_{k\sigma v} \hat{d}_{k\sigma v}, \tag{3}$$

where $\varepsilon^v_{k\sigma}$ represents the energy of the electronic states in lead v (with $v = {\rm l, r}$ for the left and right reservoirs). Here, $\hat{d}^\dagger_{k\sigma v}$ and $\hat{d}_{k\sigma v}$ are the creation and annihilation operators for electrons with wavevector k and spin σ in lead v. The leads serve as reservoirs of electrons that can tunnel into and out of the QD, facilitating transport.

The interaction between the QD and the leads is governed by the tunneling Hamiltonian, denoted as $\hat{H}_{\rm I}$, which facilitates the tunneling of electrons between the QD and the reservoirs. This term is crucial for describing the current flow through the system, as electrons can move between the QD and the left and right leads.

$$\hat{H}_{\rm I} = \sum_{k,\sigma,v={\rm l,r}} \gamma_{vk} \hat{c}^\dagger_\sigma \hat{d}_{vk\sigma} + {\rm H.c.}, \tag{4}$$

where γ_{vk} represents the coupling strength between the QD and the reservoirs. It is pertinent to note that the key parameter governing the electron–electron interaction within the quantum dot, i.e., the on-site Coulomb energy U, is experimentally highly tunable. In gate-defined semiconductor quantum dots, U can be effectively controlled by adjusting the confinement gate voltages, typically ranging from a few hundred μeV to several meV.[18,29] Similarly, in molecular transistor setups, U is a well-defined molecular property that can be selected via molecular synthesis and is often on the order of hundreds of meV. The parameter regimes explored in this work (e.g., $U \sim \mathcal{O}(1-10)$ meV) are directly accessible in these established experimental platforms, ensuring the practical relevance and testability of our theoretical predictions regarding the enhancement of thermoelectric performance and the suppression of current fluctuations.[30]

2.2. The quantum master equation with full counting statistics

Full counting statistics is widely accepted as a powerful tool for characterizing complete information about current fluctuations.[21] Based on the two-time measurement protocol,[31,32] we apply full counting statistics to obtain the particle and energy flows out of the electronic reservoirs by introducing $\chi = \{\lambda_{\rm p}, \lambda_{\rm E}\}$, respectively. Consequently, the counting-field-dependent total Hamiltonian is described as

$$H_{-\chi/2} = H_{\rm QD} + H_{\rm lead} + H_{\rm I}^{-\chi/2}, \tag{5}$$

with $H_{\rm I}^{-\chi/2}$ specified as

$$H_{\rm I}^{-\chi/2} = \sum_k (\gamma_{lk} \hat{c}^\dagger_\sigma \hat{d}_{lk\sigma}\, {\rm e}^{-{\rm i}\frac{\lambda_{\rm p}}{2} - {\rm i}\frac{\lambda_{\rm E}}{2}\varepsilon_{lk}} + \gamma_{rk} \hat{c}^\dagger_\sigma \hat{d}_{rk\sigma} + {\rm h.c.}), \tag{6}$$

where γ_{vk} represents the coupling strength between the QD and the leads, and ε_{vk} denotes the energy of electrons in lead v with wavevector k.

We assume that the dot–reservoir tunneling processes are weak. Based on the Born–Markov approximation, we perturb $V_{-\chi/2}$ to obtain the quantum master equation as[33]

$$\begin{aligned} &\frac{\partial}{\partial t}\rho_{\rm S}(\chi,t) \\ &= -{\rm i}[\rho_{\rm S}(\chi,t), H_{\rm QD}] \\ &\quad - \int_0^\infty {\rm d}\tau {\rm Tr}_{\rm B}\left\{\left[V_{-\chi/2}, \left[V_{-\chi/2}(-\tau), \rho_{\rm S}(\chi,t)\otimes\rho_{\rm B}\right]\right]\right\}, \end{aligned} \tag{7}$$

where $\rho_{\rm S}(\chi,t)$ denotes the reduced density operator of the QD system with counting parameters, i.e., $\rho_{\rm S}(\chi,t) = {\rm Tr}_{\rm B}\{\rho^{\rm T}_\chi(t)\}$,

with $\rho_\chi^{\mathrm{T}}(t)$ being the full density operator of the entire inelastic heat engine. The commutation relation is defined as $[\hat{A}_\chi, \hat{B}_\chi]_\chi = \hat{A}_\chi \hat{B}_\chi - \hat{B}_\chi \hat{A}_{-\chi}$. The equilibrium distribution of the reservoirs is specified as $\rho_{\mathrm{B}} = \rho_{\mathrm{l}} \otimes \rho_{\mathrm{r}}$, with $\rho_i = \exp\left(-\beta_i(\hat{H}_i - \mu_i \hat{N}_i)\right)/Z_i$ $(i = \mathrm{l}, \mathrm{r})$, the partition functions $Z_i = \mathrm{Tr}\left\{\exp\left(-\beta_i(\hat{H}_i - \mu_i \hat{N}_i)\right)\right\}$, and the inverse temperatures $\beta_i = 1/k_{\mathrm{B}}T_i$.

We project the quantum master equation onto the populations of the electronic levels in spin space according to $\rho_{mn} = \langle m|\rho_{\mathrm{S}}|n\rangle$, where $m, n = 0, \sigma, \bar{\sigma}, \sigma\bar{\sigma}$. If we reorganize $\rho_{\mathrm{S}}(\chi, t)$ in vector form as

$$\begin{aligned} |\boldsymbol{P}(\chi,t)\rangle\rangle = [&\langle 0|\rho_{\mathrm{S}}(\chi,t)|0\rangle; \langle\sigma|\rho_{\mathrm{S}}(\chi,t)|\sigma\rangle; \\ &\langle\bar{\sigma}|\rho_{\mathrm{S}}(\chi,t)|\bar{\sigma}\rangle; \langle\sigma\bar{\sigma}|\rho_{\mathrm{S}}(\chi,t)|\sigma\bar{\sigma}\rangle], \end{aligned}$$

the quantum master equation can be reexpressed as

$$\frac{d|\boldsymbol{P}(\chi,t)\rangle\rangle}{dt} = \boldsymbol{H}(\chi)|\boldsymbol{P}(\chi,t)\rangle\rangle, \tag{8}$$

where $\boldsymbol{H}(\chi)$ is the evolution matrix, with its elements shown in Appendix A.

To arrive at the compact form of Eq. (8), we further employ the secular approximation (also known as the rotating-wave approximation), which decouples the dynamics of populations (diagonal elements of ρ_{S}) from those of quantum coherence (off-diagonal elements). This approximation is justified when the energy scales involved in the system Hamiltonian — specifically, the level splitting $|\varepsilon_\uparrow - \varepsilon_\downarrow|$ and the Coulomb energy U — are large compared to the tunneling-induced decay rates Γ. In this regime, which is typical for Coulomb-blockaded quantum dots, the coherence elements oscillate rapidly and decay on a timescale much faster than that of the population dynamics. Therefore, for the study of steady-state transport properties, retaining only the population terms provides an excellent description of the system behavior and is a standard approach in quantum transport theory.[31,33]

This master equation governs the time evolution of the system populations, represented by the vector $\boldsymbol{P}(\chi, t)$, under the influence of the evolution matrix $\boldsymbol{H}(\chi)$. The specific elements of $\boldsymbol{H}(\chi)$ are provided in Appendix A. To enhance the physical clarity of our formulation, we include in the appendix a detailed explanation that interprets each key matrix element in terms of the underlying spin-selective tunneling processes and their modification by the Coulomb interaction U. This bridges the gap between the mathematical description and the physical tunneling events, such as electron hopping onto or off the dot, which are crucial for understanding the thermoelectric transport and fluctuation statistics discussed in the following sections.

Consequently, the particle current flowing from the left reservoir into the system is given by[28,34]

$$I_{\mathrm{e}}^{\mathrm{l}} = \frac{\partial \mathcal{G}_{\mathrm{tot}}(\chi)}{\partial(\mathrm{i}\lambda_{\mathrm{p}})}\Big|_{\chi=0}, \tag{9}$$

and the particle current from the right reservoir can be straightforwardly obtained as $I_{\mathrm{e}}^{\mathrm{r}} = -I_{\mathrm{e}}^{\mathrm{l}}$ via the law of charge conservation. Meanwhile, the energy flow is expressed as

$$I_{\mathrm{E}}^{\mathrm{l}} = \frac{\partial \mathcal{G}_{\mathrm{tot}}(\chi)}{\partial(\mathrm{i}\lambda_{\mathrm{E}})}\Big|_{\chi=0}, \tag{10}$$

and the electronic heat flow extracted from the left reservoir is defined as $I_{\mathrm{Q}}^{\mathrm{l}} = I_{\mathrm{E}}^{\mathrm{l}} - \mu_{\mathrm{l}} I_{\mathrm{e}}^{\mathrm{l}}$.[35] In analogy, the particle current $I_{\mathrm{e}}^{\mathrm{r}}$ and energy current $I_{\mathrm{E}}^{\mathrm{r}}$ flow from the right electronic reservoir into the central system.

The nonequilibrium current noise, characterizing fluctuations in particle transport, is derived as the second cumulant[8,21,36]

$$S_{\mathrm{p}} = \frac{\partial^2 \mathcal{G}_{\mathrm{tot}}(\chi)}{\partial(\mathrm{i}\lambda_{\mathrm{p}})^2}\Big|_{\chi=0}. \tag{11}$$

We analyze the operation of a heat engine that harvests energy from a hot reservoir and converts it into useful output work. The electrochemical potential bias is defined as $\Delta\mu = \mu_{\mathrm{l}} - \mu_{\mathrm{r}}$, with the average chemical potential given by $\mu \equiv (\mu_{\mathrm{l}} + \mu_{\mathrm{r}})/2$. The useful output power of the heat engine is expressed as

$$P_{\mathrm{out}} = I_{\mathrm{e}}^{\mathrm{l}} \cdot \Delta\mu. \tag{12}$$

The total entropy production of the system is given by $\dot{S}_{\mathrm{tot}} = -\sum_{v=\mathrm{l},\mathrm{r}} I_{\mathrm{Q}}^{v}/T_v$,[20] which can be further expressed in the specific form

$$T_{\mathrm{l}}\dot{S}_{\mathrm{tot}} = \left(1 - \frac{T_{\mathrm{l}}}{T_{\mathrm{r}}}\right) I_{\mathrm{Q}}^{\mathrm{r}} - P_{\mathrm{out}}. \tag{13}$$

From Eq. (13), it is evident that the thermodynamic device can function as a quantum heat engine and generate useful work even in the absence of a temperature gradient. Notably, when the electric power satisfies $P_{\mathrm{out}} > 0$, the device operates as a heat engine. The efficiency of the heat engine is given by

$$\eta = \frac{P_{\mathrm{out}}}{\left(1 - \frac{T_{\mathrm{l}}}{T_{\mathrm{r}}}\right) I_{\mathrm{Q}}^{\mathrm{r}}}, \tag{14}$$

and is bounded by the Carnot efficiency $\eta_C = 1 - T_{\mathrm{l}}/T_{\mathrm{r}}$ due to the second law of thermodynamics.[37–39]

3. Results and discussions

3.1. Thermodynamic performance of the thermoelectric heat engines

Figure 2 presents the key thermodynamic characteristics of our QD heat engine system. Figures 2(a) and 2(b) respectively demonstrate the evolution of the output power P_{out} and the normalized efficiency η/η_{C} as functions of the chemical potential difference $\Delta\mu$ for different electron–electron interaction strengths U. The results reveal two significant trends. Figure 2(a) clearly shows that stronger electron–electron interactions lead to substantially improved power generation. Under identical parameter conditions, the output power exhibits a

progressive enhancement with increasing values of U. Correspondingly, the energy conversion efficiency shows a similar enhancement for stronger Coulomb interactions, as evidenced in Fig. 2(b). This simultaneous improvement in both output power and efficiency indicates that electron–electron interaction effects play a crucial role in optimizing the thermoelectric performance of QD systems. The observed behavior can be physically understood through the interplay between Coulomb blockade effects and thermoelectric transport. Stronger values of U modify the available transport channels and the energy-dependent transmission properties, leading to more favorable conditions for harvesting energy from the temperature gradient.

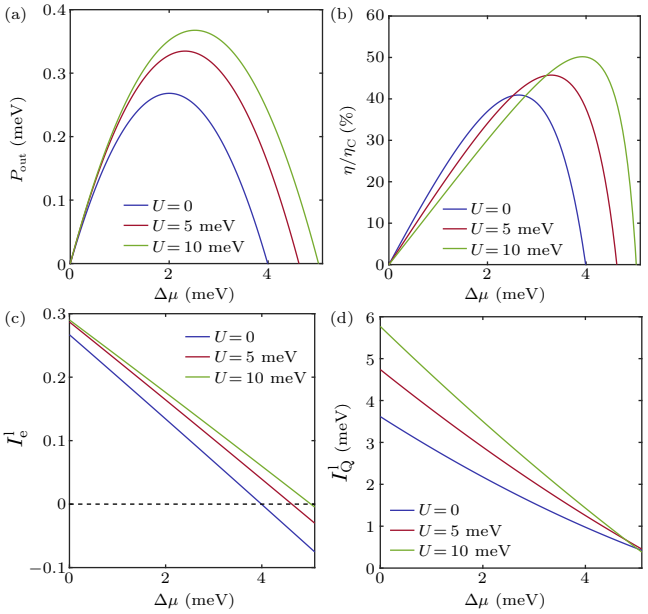


Fig. 2. (a) The output power $P_{\rm out}$, (b) the efficiency $\eta/\eta_{\rm C}$, (c) the electronic current $I_{\rm e}^{\rm l}$, and (d) the heat current $I_{\rm Q}^{\rm l}$ as functions of $\Delta\mu$ for different electron–electron interaction strengths U. The parameters are $k_{\rm B}T_{\rm l}=10$ meV, $k_{\rm B}T_{\rm r}=15$ meV, $\mu=0$, $\Gamma_{\rm l}=\Gamma_{\rm r}=4$ meV, $\varepsilon_{\uparrow}=16$ meV, and $\varepsilon_{\downarrow}=4$ meV.

To further elucidate the mechanism behind the enhanced heat engine performance, we examine the behavior of both electrical and heat currents as functions of the chemical potential difference $\Delta\mu$, as shown in Figs. 2(c) and 2(d). The improvement in output power directly correlates with the Coulomb-interaction-induced enhancement of the electrical current (Fig. 2(c)). Stronger electron–electron interactions yield significantly increased current flow through the QD system. While both the electronic current (Fig. 2(c)) and the heat current (Fig. 2(d)) increase with U, their relative growth rates differ. Notably, in the regime $\Delta\mu \leq 2$ meV, the system exhibits higher efficiency in the absence of Coulomb interactions ($U=0$) compared to interacting cases. This suggests that the interaction-enhanced heat current partially offsets the power gain, and a crossover occurs where interaction effects become beneficial only beyond certain potential differences. These observations highlight the delicate balance between current enhancement and thermal management in optimizing quantum thermoelectric systems. The non-monotonic dependence of the efficiency on the interaction strength indicates the existence of optimal operating conditions that depend on both the potential bias and interaction parameters.

3.2. Fluctuation characteristics in QD heat engines

In nanoscale quantum systems, the study of current fluctuations provides a crucial window into quantum thermodynamic processes. While the average current $I_{\rm e}^{\rm l}$ characterizes the steady-state charge transport, the current noise $S_{\rm p}$, defined as the zero-frequency component of the current–current correlation function, reveals fundamental information about the granularity of transport and electron correlations. Investigating fluctuations is therefore essential for understanding the full statistics of quantum transport and for assessing the stability and potential signal-to-noise ratio of nanoelectronic devices, such as quantum thermoelectric converters.

In Fig. 3(a), we first present the current noise $S_{\rm p}$ as a function of the chemical potential difference $\Delta\mu$, revealing several important features. It shows a systematic reduction in the current noise with increasing electron–electron interaction strength U. This clear anti-correlation between $S_{\rm p}$ and U indicates that Coulomb interactions effectively suppress fluctuations in quantum thermoelectric transport.

To further characterize the noise properties, we examine the Fano factor F, defined as the ratio of the current noise to the average current[3]

$$F \equiv \frac{S_{\rm p}}{|I_{\rm e}^{\rm l}|}. \tag{15}$$

As shown in Fig. 3(b), F decreases monotonically with increasing Coulomb interaction strength U, which is consistent with the suppression of the absolute noise $S_{\rm p}$ observed in Fig. 3(a). This consistent trend across both absolute and normalized measures of noise robustly confirms that electron correlations play a crucial role in stabilizing charge transport through the quantum dot. The physical mechanism underlying this fluctuation suppression can be understood as follows. Enhanced Coulomb repulsion inhibits simultaneous multi-electron tunneling events due to the large energy cost of double occupancy. Consequently, stronger interactions effectively narrow the available transport channels, enforcing a more regular, sequential flow of electrons. This transition toward a more ordered transport regime is directly reflected in the reduction of the shot noise. The simultaneous decrease in both $S_{\rm p}$ and F signifies that Coulomb interactions not only suppress the absolute magnitude of current fluctuations but also enhance the signal-to-noise ratio of the thermoelectric current. This property is particularly valuable for applications that demand stable performance from nanoscale energy conversion devices.

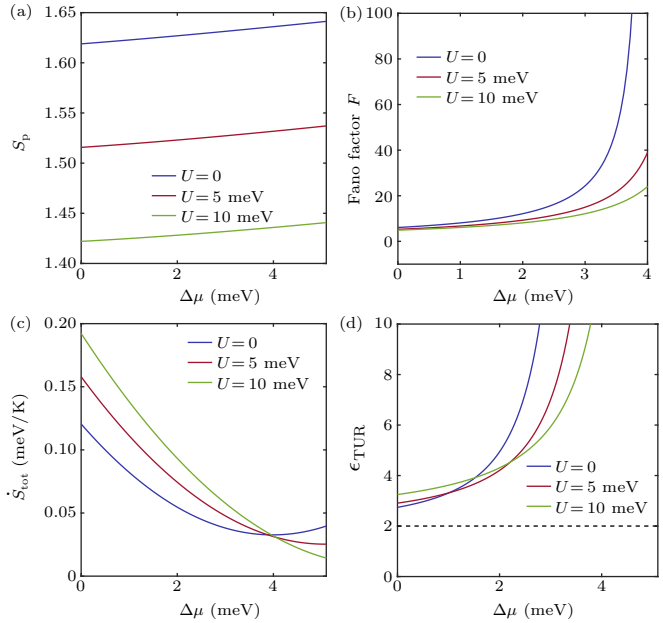


Fig. 3. (a) The noise S_p of the electronic current, (b) the Fano factor, (c) the entropy production rate $\dot{S}_{tot}$, and (d) the TUR relation as functions of $\Delta\mu$ for different electron–electron interaction strengths U. The other parameters are the same as those in Fig. 2.

Recent advances in stochastic thermodynamics have revealed a fundamental TUR for classical Markovian systems at steady state,[23,24] establishing an intrinsic trade-off between current fluctuations and entropy production. This relation constrains the relative current fluctuations through the inequality

$$\varepsilon_{TUR} \equiv \frac{S_p}{(I_e^l)^2}\dot{S}_{tot} \geq 2. \tag{16}$$

The TUR provides critical insights into nonequilibrium thermodynamics by quantifying the fundamental limit on precision in terms of thermodynamic dissipation. Originally derived at steady state,[23,25,26] this relation has subsequently been extended to the finite-time regime.[27,28]

Our QD system offers an ideal platform to examine how strong electron correlations affect this fundamental thermodynamic bound. Specifically, Fig. 3(c) presents the entropy production rate $\dot{S}_{tot}$ under varying Coulomb interaction strengths, while Fig. 3(d) explicitly tests the validity of the TUR through the parameter ε_{TUR}. Our results reveal that the thermodynamic uncertainty relation remains rigorously valid ($\varepsilon_{TUR} \geq 2$) across all interaction strengths, demonstrating remarkable robustness even under strong Coulomb interactions up to $U =$ 10 meV. Notably, the interaction strength systematically modulates ε_{TUR}, driving it closer to the bound while simultaneously increasing its minimum value — a distinct departure from classical non-interacting systems, where ε_{TUR} typically saturates at 2. This behavior suggests that electron correlations impose additional constraints on current fluctuations beyond standard TUR predictions.

The observed validity of the TUR can be traced to the Lindblad form of our quantum master equation, which results from the secular approximation. It has been established that such a Lindblad form inherently guarantees the validity of the TUR at steady state.[24] Therefore, our results not only affirm the thermodynamic consistency of strongly correlated quantum systems but also demonstrate the robustness of this fundamental bound within a well-defined Lindblad dynamical framework. This provides a deeper theoretical context for our findings and confirms the broader applicability of thermodynamic uncertainty relations in the quantum regime, with important implications for the design of quantum thermal machines.

4. Conclusion

In this work, we have systematically and carefully investigated the thermoelectric and fluctuation properties of a Coulomb-blockaded QD system operating as a highly efficient nanoscale heat engine. Through comprehensive theoretical analysis and detailed numerical calculations, several key findings have been firmly established. First, we demonstrated that electron–electron interactions significantly enhance the thermoelectric performance, with both the output power and energy conversion efficiency showing marked improvement with increasing Coulomb interaction strength U. This enhancement originates from interaction-induced modifications of transport channels and more favorable energy-dependent transmission properties. Second, our analysis of current fluctuations revealed that Coulomb interactions play a crucial role in effectively suppressing quantum noise. Both the absolute current noise and the Fano factor exhibit systematic reduction with stronger interactions, indicating that electron correlations can effectively stabilize charge transport in realistic nanoscale thermoelectric devices. Most importantly, we examined the validity of the TUR in this strongly correlated quantum system. Despite the presence of significant Coulomb interactions, the TUR remains rigorously satisfied, demonstrating the remarkable robustness of this fundamental thermodynamic bound even in the quantum regime. However, the interaction-dependent behavior of ε_{TUR} suggests that electron correlations may introduce additional important constraints beyond those captured by classical formulations of the TUR.

The insights gained from our work provide clear guidance for future experimental efforts aimed at optimizing advanced quantum thermoelectric devices.[16] Specifically, our results suggest that operating in the strong Coulomb-blockade regime and utilizing quantum dots with sizable electron–electron interactions are highly promising pathways to achieve simultaneously high power output, superior efficiency, and stabilized current flow. The predicted interplay between interaction strength and fluctuation suppression offers a clearly testable signature for future experiments focusing on the noise properties of nanoscale heat engines.

Appendix A: The elements of the evolution matrix

If we reorganize $\rho_{\rm S}(\chi,t)$ in vector form as $|\boldsymbol{P}(\chi,t)\rangle\rangle = [\langle 0|\rho_{\rm S}(\chi,t)|0\rangle;\ \langle\sigma|\rho_{\rm S}(\chi,t)|\sigma\rangle;\ \langle\bar{\sigma}|\rho_{\rm S}(\chi,t)|\bar{\sigma}\rangle;\ \langle\sigma\bar{\sigma}|\rho_{\rm S}(\chi,t)|\sigma\bar{\sigma}\rangle]^{\rm T}$, the quantum master equation can be re-expressed as

$$\frac{{\rm d}|\boldsymbol{P}(\chi,t)\rangle\rangle}{{\rm d}t} = \boldsymbol{H}(\chi)|\boldsymbol{P}(\chi,t)\rangle\rangle, \tag{A1}$$

where $\boldsymbol{H}(\chi)$ is the evolution matrix, with its elements given as

$$\boldsymbol{H}(\chi,t) = \begin{pmatrix} H_{11} & H_{12} & H_{13} & H_{14} \\ H_{21} & H_{22} & H_{23} & H_{24} \\ H_{31} & H_{32} & H_{33} & H_{34} \\ H_{41} & H_{42} & H_{43} & H_{44} \end{pmatrix}, \tag{A2}$$

where the matrix elements are defined as follows:

$$\begin{aligned}
H_{11} &= -\sum_{\sigma,v={\rm l,r}} \Gamma_\sigma^v f_v(\varepsilon_\sigma),\\
H_{12} &= \Gamma_\uparrow^{\rm l} {\rm e}^{+{\rm i}\lambda_{\rm p}+{\rm i}\lambda_{\rm E}(\varepsilon_\uparrow+U)}(1-f_{\rm l}(\varepsilon_\uparrow)) + \Gamma_\uparrow^{\rm r}(1-f_{\rm r}(\varepsilon_\uparrow)),\\
H_{13} &= \Gamma_\downarrow^{\rm l} {\rm e}^{+{\rm i}\lambda_{\rm p}+{\rm i}\lambda_{\rm E}(\varepsilon_\downarrow+U)}(1-f_{\rm l}(\varepsilon_\downarrow)) + \Gamma_\downarrow^{\rm r}(1-f_{\rm r}(\varepsilon_\downarrow)),\\
H_{14} &= 0,\\
H_{21} &= \Gamma_\uparrow^{\rm l} {\rm e}^{-{\rm i}\lambda_{\rm p}-{\rm i}\lambda_{\rm E}(\varepsilon_\uparrow+U)} f_{\rm l}(\varepsilon_\uparrow) + \Gamma_\uparrow^{\rm r} f_{\rm r}(\varepsilon_\uparrow),\\
H_{22} &= -\sum_{v={\rm l,r}} \Gamma_\uparrow^v(1-f_v(\varepsilon_\uparrow)) - \sum_{v={\rm l,r}} \Gamma_\downarrow^v f_v(\varepsilon_\downarrow+U),\\
H_{23} &= 0,\\
H_{24} &= \Gamma_\downarrow^{\rm l} {\rm e}^{+{\rm i}\lambda_{\rm p}+{\rm i}\lambda_{\rm E}\varepsilon_\downarrow}(1-f_{\rm l}(\varepsilon_\downarrow+U)) + \Gamma_\downarrow^{\rm r}(1-f_{\rm r}(\varepsilon_\downarrow+U)),\\
H_{31} &= \Gamma_\downarrow^{\rm l} {\rm e}^{-{\rm i}\lambda_{\rm p}-{\rm i}\lambda_{\rm E}(\varepsilon_\downarrow+U)} f_{\rm l}(\varepsilon_\downarrow) + \Gamma_\downarrow^{\rm r} f_{\rm r}(\varepsilon_\downarrow),\\
H_{32} &= 0,\\
H_{33} &= -\sum_{v={\rm l,r}} \Gamma_\downarrow^v(1-f_v(\varepsilon_\downarrow)) - \sum_{v={\rm l,r}} \Gamma_\uparrow^v f_v(\varepsilon_\uparrow+U),\\
H_{34} &= \Gamma_\uparrow^{\rm l} {\rm e}^{+{\rm i}\lambda_{\rm p}+{\rm i}\lambda_{\rm E}\varepsilon_\uparrow}(1-f_{\rm l}(\varepsilon_\uparrow+U)) + \Gamma_\uparrow^{\rm r}(1-f_{\rm r}(\varepsilon_\uparrow+U)),\\
H_{41} &= 0,\\
H_{42} &= \Gamma_\downarrow^{\rm l} {\rm e}^{-{\rm i}\lambda_{\rm p}-{\rm i}\lambda_{\rm E}\varepsilon_\downarrow} f_{\rm l}(\varepsilon_\downarrow+U) + \Gamma_\downarrow^{\rm r} f_{\rm r}(\varepsilon_\downarrow+U),\\
H_{43} &= \Gamma_\uparrow^{\rm l} {\rm e}^{-{\rm i}\lambda_{\rm p}-{\rm i}\lambda_{\rm E}\varepsilon_\uparrow} f_{\rm l}(\varepsilon_\uparrow+U) + \Gamma_\uparrow^{\rm r} f_{\rm r}(\varepsilon_\uparrow+U),\\
H_{44} &= -\sum_{\sigma,v={\rm l,r}} \Gamma_\sigma^v(1-f_v(\varepsilon_\sigma+U)).
\end{aligned} \tag{A3}$$

The evolution matrix $\boldsymbol{H}(\chi,t)$ satisfies the detailed balance condition

$$\frac{H_{ij}}{H_{ji}} = \frac{P_j^{\rm eq}}{P_i^{\rm eq}} = {\rm e}^{-\beta(E_j-E_i)} \tag{A4}$$

for all pairs of states (i,j), where $P_i^{\rm eq}$ denotes the equilibrium population of state i and E_i represents its energy. This condition can be verified by examining all nonzero transition rates in the matrix and confirming that they obey the Boltzmann ratio at equilibrium.

Acknowledgments

This project was supported by the National Natural Science Foundation of China (Grant No. 12305050), the Natural Science Foundation of Jiangsu Higher Education Institutions of China (Grant No. 23KJB140017), and the Zhejiang Provincial Natural Science Foundation of China (Grant No. LZ25A050001).

References

[1] Benenti G, Casati G, Saito K and Whitney R S 2017 *Phys. Rep.* **694** 1
[2] Maria Cangemi L, Bhadra C and Levy A 2024 *Phys. Rep.* **1087** 1
[3] Landi G T and Paternostro M 2021 *Rev. Mod. Phys.* **93** 035008
[4] Wang R, Wang C, Lu J and Jiang J H 2022 *Adv. Phys. X* **7** 2082317
[5] Jiang J H, Entin-Wohlman O and Imry Y 2012 *Phys. Rev. B* **85** 075412
[6] Lu J, Wang R, Liu Y and Jing J H 2017 *J. Appl. Phys.* **122** 044301
[7] Liu Y, Lu J, Wang R, Wang C and Jiang J H 2020 *Chin. Phys. B* **29** 40504
[8] Lu J, Liu J, Jiang J H and Wang C 2025 *Phys. Rev. B* **111** 245407
[9] Sanchez R and Büttiker M 2011 *Phys. Rev. B* **83** 085428
[10] Sanchez R, Sothmann B and Jordan A N 2015 *Phys. Rev. Lett.* **114** 146801
[11] Liu D, Yuan J, Ruan H, Xu Y, Luo S, He J, He X, Ma Y and Wang J H 2024 *Phys. Rev. A* **110** 042218
[12] Liu D, Hong Y, Luo S, He X, Wu Z and Wang J 2025 *Phys. Rev. A* **111** 012203
[13] Xu Y, Ruan H, Luo S, Guo S, He X and Wang J 2025 *Phys. Rev. E* **111** L022101
[14] Ren J, Zhu J X, Gubernatis J E, Wang C and Li B 2012 *Phys. Rev. B* **85** 155443
[15] Yang J, Elouard C, Splettstoesser J, Sothmann B, Sanchez R and Jordan A N 2019 *Phys. Rev. B* **100** 045418
[16] Thierschmann H, Sanchez R, Sothmann B, Buhmann H and Molenkamp L W 2016 *C. R. Phys.* **17** 1109
[17] Xi M, Wang R, Lu J and Jiang J H 2021 *Chin. Phys. Lett.* **38** 088801
[18] Thierschmann H, Arnold F, Mittermüller M, Maier L, Heyn C, Hansen W, Buhmann H and Molenkamp L W 2015 *New J. Phys.* **17** 113003
[19] Lu J, Wang R, Wang C and Jiang J H 2023 *Entropy* **25** e25030498
[20] Lu J, Wang Z, Wang R, Peng J, Wang C and Jiang J H 2023 *Phys. Rev. B* **107** 075428
[21] Lu J, Wang Z, Ren J, Wang C and Jiang J H 2024 *Phys. Rev. B* **109** 125407
[22] Cao B, Han C, Hao X, Wang C and Lu J 2024 *Chin. Phys. Lett.* **41** 077302
[23] Barato A C and Seifert U 2015 *Phys. Rev. Lett.* **114** 158101
[24] Horowitz J M and Gingrich T R 2020 *Nat. Phys.* **16** 15
[25] Liu J and Segal D 2019 *Phys. Rev. E* **99** 062141
[26] Liu J and Segal D 2021 *Phys. Rev. E* **103** 032138
[27] Van Vu T and Hasegawa Y 2020 *Phys. Rev. Research* **2** 013060
[28] Lu J, Wang Z, Peng J, Wang C, Jiang J H and Ren J 2022 *Phys. Rev. B* **105** 115428
[29] Thierschmann H, Sanchez R, Sothmann B, Arnold F, Heyn C, Hansen W, Buhmann H and Molenkamp L W 2015 *Nat. Nanotech.* **10** 854
[30] Willing S, Lehmann H, Volkmann M and Klinke C 2017 *Sci. Adv.* **3** e1603191
[31] Esposito M, Harbola U and Mukamel S 2009 *Rev. Mod. Phys.* **81** 1665
[32] Campisi M, Hänggi P and Talkner P 2011 *Rev. Mod. Phys.* **83** 771
[33] Breuer H P and Petruccione F 2002 *The Theory of Open Quantum Systems* (Oxford: Oxford University Press)
[34] Agarwalla B K, Jiang J H and Segal D 2017 *Phys. Rev. B* **96** 104302
[35] Lu J, Liu Y, Wang R, Wang C and Jiang J H 2019 *Phys. Rev. B* **100** 115438
[36] Landi G T, Kewming M J, Mitchison M T and Potts P P 2024 *PRX Quantum* **5** 020201
[37] Jiang J H 2014 *Phys. Rev. E* **90** 042126
[38] Wang R, Lu J, Wang C and Jiang J H 2018 *Sci. Rep.* **8** 2607
[39] Liu J, Jung K A and Segal D 2021 *Phys. Rev. Lett.* **127** 200602